IOP PUBLISHING CLASSICAL AND QUANTUM GRAVITY

Class. Quantum Grav. **25** (2008) 235013 (12pp) doi:10.1088/0264-9381/25/23/235013

Development of a signal-extraction scheme for resonant sideband extraction

K Kokeyama[1], K Somiya[2], F Kawazoe[1], S Sato[3], S Kawamura[3] and A Sugamoto[1]

[1] Graduate School of Humanities and Sciences, Ochanomizu University, 2-1-1, Otsuka, Bunkyo-ku, Tokyo 112-8610, Japan
[2] Max-Planck-Institut für Gravitationsphysik, Am Mühlenberg 1, 14476 Potsdam, Germany
[3] National Astronomical Observatory of Japan, 2-21-1, Osawa, Mitaka, Tokyo 181-8588, Japan

E-mail: keiko.kokeyama@nao.ac.jp

Received 2 June 2008, in final form 25 August 2008
Published 17 November 2008
Online at stacks.iop.org/CQG/25/235013

Abstract

As a future plan, an advanced gravitational-wave detector will employ an optical configuration of resonant sideband extraction (RSE), achieved with an additional mirror at the signal-detection port of the power-recycled Fabry–Perot Michelson interferometer. To control the complex coupled cavity system, one of the most important design issues is how to extract the longitudinal control signals of the cavities. We have developed a new signal-extraction scheme which provides an appropriate sensing matrix. The new method uses two sets of sidebands: one of the sideband components satisfies the critical coupling condition for the RSE interferometer and reaches the signal-extraction port, and the other sideband is completely reflected by the Michelson interferometer. They provide a diagonalized sensing matrix and enable the RSE control to be robust.

PACS numbers: 04.80.Nu, 42.60.Da, 95.55.Ym

(Some figures in this article are in colour only in the electronic version)

1. Introduction

Gravitational-wave detection will provide evidence of the most important part of Einstein's general theory of relativity and will start a new era of observational astronomy.

Gravitational waves are the ripples of spacetime that travel through space. They have extremely little interaction with matter, but they cause the differential displacement of free masses. Around the world, several interferometric gravitational-wave observatories aim at

the first detection of gravitational waves. The ground-based gravitational-wave antennas are based on a Michelson interferometer (MI) with a stabilized laser. When the gravitational-waves pass, they will produce a differential length change of the interferometer's arms. The displacement will be detected as a relative phase change of these two arms. However, the magnitude of the displacement measured by the detectors is so small, only about 10^{-20} m, even for large scale detectors, that the sensitivity is disturbed by various kinds of noise. Toward the achievement of extremely high sensitivity, several optical configurations and various noise reduction techniques have been developed. But so far, no attempt to directly detect gravitational waves has been successful.

The first-generation detectors such as TAMA300 [1], VIRGO [2], GEO 600 [3] and LIGO [4, 5] have been constructed and are currently in operation. The power-recycled Fabry–Perot (FP) Michelson interferometer is employed as the optical configuration for most of these detectors. Two FP resonant cavities are placed to increase the light storage time and enhance the gravitational-wave signals. In a simple MI case, the interferometer is kept on a dark fringe at the dark port to optimize the shot-noise-limited sensitivity and all the carrier light will return to the laser and will be wasted. To utilize these lights effectively, a power-recycling mirror (PRM) is placed in front of the MI so that the effective laser power is increased in the interferometer. Although these detectors are in the process of reaching a remarkable sensitivity, current-operating detectors can detect gravitational-wave events only in the range of about 15 Mpc at the maximum. This is not enough to establish gravitational-wave astronomy.

More sensitive second generation detectors are being planned and developed. The Japanese future plan, the Large Cryogenic Gravitational-wave Telescope (LCGT) [6] and the US plan, Advanced LIGO [7], are undergoing development as the second-generation gravitational-wave detectors. Their sensitivities will improve with various new techniques such as very high power laser, advanced suspension systems, cryogenics, new optical configurations, etc. As one of these advanced techniques, the resonant sideband extraction (RSE) [8] is selected as the standard optical configuration of these future detectors.

The RSE topology requires an additional mirror at the dark port. However, this mirror adds another longitudinal degree of freedom to control and makes its optical configuration complex. Therefore, it is essential to have a length-sensing scheme suitable for the RSE interferometer.

In the following section, we will review the RSE interferometer, in particular, focusing on its optical configuration. Then we will propose a new length-sensing scheme in section 3, and explain how it developed in section 4. In section 5, we will show the simulation result and the discussion. At the end, we will summarize our work.

2. Length sensing of RSE

The optical configuration of the RSE interferometer is shown in figure 1. The interferometric part consists of two input test masses and a beam splitter (BS). An input test mass and an end test mass form an FP cavity which plays an important role in the gravitational-wave signal enhancement. Additionally, the interferometer also has a PRM at the bright port (BP)[4] and a signal extraction mirror (SEM) at the dark port (DP). The carrier field resonates inside both arm cavities and the power-recycling cavity (PRC). This is the so-called tuned RSE configuration, which is the default plan for LCGT.

Since the arm cavities have a high finesse (which indicates how many round trips light travels in a cavity) in the RSE configuration, the gravitational-wave signals are enhanced

[4] These ports are traditionally called dark and bright, although they are not bright or dark for an RSE interferometer.

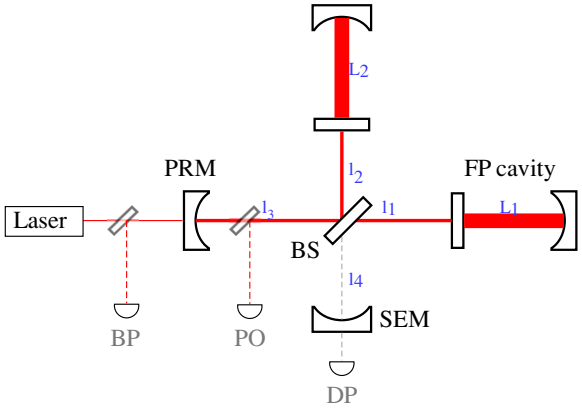

Figure 1. Optical configuration of RSE. Two FP cavity lengths are L_1 and L_2. The MI has two light paths of lengths l_1 and l_2. l_3 is the distance from the PRM to the BS and l_4 is that from the BS to the SEM. There are three detection ports for length-sensing: the BP, the DP and the PO.

accordingly. However, the signals are over-circulated and they are canceled in the arm cavity owing to the phase changes of the gravitational-wave signals. The SEM plays an important role in circumventing this problem. The signal extraction cavity (SEC) lowers the effective finesse for the gravitational-wave signals and they escape from the cavities before over-circulation. On the other hand, the entire carrier light returns to the BP, so the SEC does not affect the power in the arm cavities. Thus the sensitivity will be improved.

The advantage of the RSE configuration is that the thermal problems can be circumvented by being compared with an optical configuration of FP MI with a PRC, which has the same sensitivity. The light power at the beam splitter or at the PRC is lower in the RSE case than in the FP MI case with a PRC. Especially for the LCGT, the mirrors will be kept at a super cryogenic temperature, thus it is necessary that the heat produced by the laser light absorption in the bulk of the input test masses is released through the suspension systems. If the heat is too high, the suspension systems cannot be refrigerated. Furthermore, the thermal lens effect may occur even if the beam splitter and the PRM are cooled. It would disrupt the mode matching of the light field and decrease the power in the arm cavities, possibly leading to a worse shot noise limit.

To operate the interferometer as a gravitational-wave detector, all the mirrors have to be controlled at the proper positions so that the cavities are on resonance for the light fields. The longitudinal signals should be sent to the mirrors to control their positions. For the RSE interferometer, as shown in figure 1, there are five degrees of freedom to control; the arm-length common mode L_+, the differential mode L_-, the PRC length l_+, the MI differential length l_- and the SEC length l_s. The exact definitions of these lengths are shown in table 1.

L_+ and L_- signals are extracted relatively independently since the phase sensitivities are enhanced by its stored light fields in the high finesse arm cavities. The difficulty is to extract the three signals of the central part of the RSE. If there is no cross-talk between these signals, only one signal component can be sent and fed back to one degree of freedom most appropriately. In this ideal control condition, the system will be very robust. However, in most of the control schemes currently used or planned for use, these three signals are mixed with the others.

Table 1. Five longitudinal degrees of freedom of the RSE. L_1 and L_2 denote the inline and perpendicular arm lengths. l_1 and l_2 are the inline and perpendicular path lengths of an MI. $\bar{l} = (l_1 + l_2)/2$; the average light path length of MI. l_3 and l_4 designate the distance from the PRM to the BS, and from the SEM to the BS. They are also found in figure 1.

Description	Symbol	Length
Common arm cavity	L_+	$L_1 + L_2$
Differential arm cavity	L_-	$L_1 - L_2$
PRC length	l_+	$l_3 + \bar{l}$
Differential MI	l_-	$l_1 - l_2$
SEC length	l_s	$l_4 + \bar{l}$

3. Coupled-reflected method

3.1. Definition of the coupled-reflected method

Our scheme, the *critically coupled-reflected method* (*coupled-reflected method* for short) employs two sets of rf sidebands which do not enter the arm cavities to prevent the admixture of the arm length signals (L_+ and L_-) and the other signals (l_+, l_- and l_s). In the conventional way, L_+ and L_- signals are extracted by beating between the carrier light and PM sidebands at the BP and DP, respectively. To obtain l_+, l_- and l_s signals, the two sets of sidebands are double-demodulated at the PO. This technique requires that one of the two sidebands is phase-modulated whereas the other sideband is amplitude-modulated to be a local field against the PM field on the double demodulation scheme. The resonant conditions of the two sets of sidebands are:

(i) The PM sidebands satisfy the critical coupling condition. The critical coupling condition requires that the reflectivity of the PRM and the reflectivity of the compound mirror which consists of the MI and SEC be equal (explained later). The PM sidebands are resonant both inside the PRC and the SEC, and carry information of the SEC effectively [11].

(ii) The AM sidebands are reflected completely by the MI so as not to carry any information of the SEC length. This condition can prevent a complex mixture between l_s and l_+.

(iii) The AM sideband is the applied so-called delocation scheme. Delocation is the macroscopic detuning of AM sidebands by a slight change in the PRM position [9]. The length-sensing matrix can be diagonalized by this delocation scheme.

The pair of sideband frequencies has to be determined to satisfy conditions (i) and (ii). To make the issue less complicated, let us introduce a view of the RSE interferometer as a coupled-cavity system. The central part of the RSE interferometer can be modeled by a coupled cavity which contains three mirrors (see figure 2).

The reflectivity of the middle compound mirror (which corresponds to the MI), r_{MI}, can be determined by choosing the MI asymmetry length $\Delta\ell$, and the sideband frequency, f_j:

$$r_{\mathrm{MI}\,j} = \cos\alpha_j \tag{1}$$

$$\alpha_j = \frac{\Delta\ell 2\pi f_j}{c}, \tag{2}$$

where $j = 1, 2$ for the PM and AM sidebands respectively. The reflectivities of the arm cavities are assumed to be unity since neither of the sidebands go into the cavities.

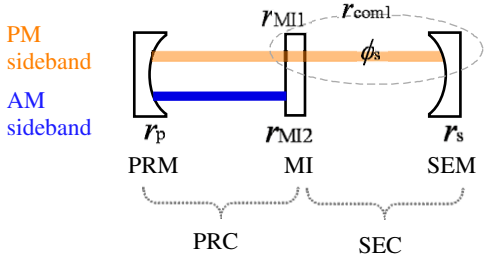

Figure 2. An RSE interferometer can be modeled by a coupled cavity which contains the PRM (reflectivity r_p), the MI and the SEM (reflectivity r_s). The former cavity corresponds to the PRC, and the second one corresponds to the section, r_{MI1} and r_{MI2} are the reflectivities of the MI for the PM and AM sidebands respectively. r_{com1} is the reflectivity of the compound mirror composed of the MI and the SEM, for the PM sideband.

We shall consider that the middle mirror and the SEM make another compound mirror again. The reflectivity of the new compound mirror is

$$r_{com\,j} = \cos\alpha_j - \frac{r_s \sin^2\alpha_j \, e^{i\phi_{sj}}}{1 - r_s \cos\alpha_j \, e^{i\phi_{sj}}}, \tag{3}$$

where ϕ_{sj} is the round trip phase between the middle mirror and the SEM.

(i) To determine the PM sideband frequency, f_1.
f_1 satisfy the critical coupling condition. In general, critical coupling is achieved when the input and end mirror have the same reflectivity and the laser lights are resonant in the cavity. The laser fields pass through the cavity without returning to the input port. To apply this condition for f_1 to the RSE interferometer, the PRM and the compound mirror which consists of the MI and SEM have the same reflectivity. Therefore, the reflectivity of the compound mirror satisfies

$$r_{com1} = r_p. \tag{4}$$

f_1 should be resonant in the SEC, $e^{i\phi_{s1}} = 1$. Substituting these conditions into equation (3), we get

$$f_1 = \frac{c}{2\pi\Delta\ell}\cos^{-1}\left(\frac{r_p + r_s}{r_p r_s + 1}\right). \tag{5}$$

To realize the resonant condition in the PRC, f_1 should also satisfy

$$f_1 = \left(N + \tfrac{1}{2}\right)\nu_{PRC}, \tag{6}$$

where ν_{PRC} is the free spectral range (FSR) of the PRC, which is $\nu_{PRC} = c/2\ell_{PRC}$ and N is an arbitrary integer. This is because the sign of the carrier field is inverted by coming back from the two arm cavities, and they are resonant in the PRC when the PRC length is the anti-resonant condition for the carrier light (see, figure 3(*a*)). In a similar way, f_1 also satisfies

$$f_1 = N' \times \nu_{SEC}, \tag{7}$$

where ν_{SEC} is the FSR of the SEC and N' is an arbitrary integer. As is shown in figure 3(*b*), the SEC cavity length is set as the resonant for the carrier light. With this condition, the carrier light is virtually anti-resonant in the SEC because the carrier light comes back from the arm cavities.

(*a*) in the PRC

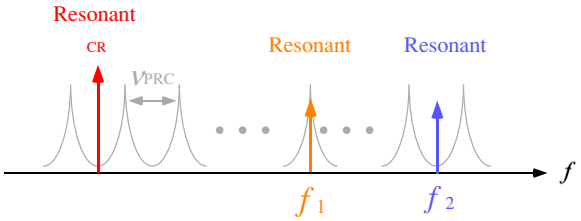

(*b*) in the SEC

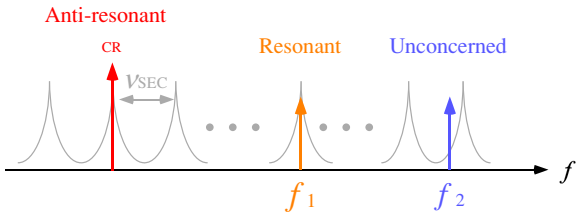

Figure 3. Relation between the cavity FSRs and the sideband frequencies. (a) PRC transmission curve. The FSR of the PRC is ν_{PRC}. The carrier light (CR) is resonant since the sign is flipped by the arm cavities. The PM sidebands (f_1) are resonant. The AM sidebands (f_2) are resonant since the sign is flipped by $r_{MI2} = -1$. (b) SEC transmission curve. The FSR of the SEC is ν_{SEC}. The carrier light is anti-resonant. The PM sidebands are resonant. The AM sidebands do not depend on ν_{SEC} since it does not enter the cavity.

(ii) To determine the AM sideband frequency, f_2.
To make the AM sidebands be reflected by the MI, $r_{MI2} = \pm 1$. Here, we supposed $r_{MI2} = -1$ to make f_2 as low as possible. Therefore the AM sideband frequency satisfies

$$f_2 = \frac{c}{2\Delta\ell}. \tag{8}$$

In addition, f_2 also satisfies

$$f_2 = \nu_{PRC} \times N'' \tag{9}$$

to be resonant in the PRC. N'' is an arbitrary integer. This is because the sign of the AM sideband fields is inverted by $r_{MI2} = -1$.

Practically, when we design a interferometer, a so-called mode cleaner between the modulators and the interferometer will be necessary to eliminate the higher order Gaussian modes of the laser light. In order for both sets of sidebands and the carrier light to transmit through the mode cleaner, the values of f_1 and f_2 should be integer multiples of the FSR of the mode cleaner cavity. However, under this additional condition, f_1 and f_2 cannot satisfy equations (6) and (9) at the same time. Therefore, in practical ways, we may use the values which satisfy the above conditions approximately and do not disturb the optical conditions.

This is one challenge of this method. The suitable optical parameters are discrete and not flexible for the changes of interferometer design because the parameters such as mirror reflectivities, the asymmetry length of MI and sideband frequencies depend on the optical design.

3.2. Features of the coupled-reflected method

One of the advantages of the coupled-reflected method is that a short asymmetry length can be achieved. The short asymmetry lengths are utilized for current gravitational-wave detectors

and can avoid any risks that might occur by changing from the current optical layout. The latent problems caused by long asymmetry lengths are phase noises and mode matching. When the inline and perpendicular paths have a long asymmetry length, laser phase noises may not be canceled by each other at the detection port. And also, the mode mismatch because of the long asymmetry length may cause the optical losses. We note that this mode mismatch can be compensated for by accommodating mirror curvatures in principle.

As a difficulty, the frequency f_2 tends to be high due to a very short asymmetry length (see equation (8)), though the AM sideband is not the local oscillator for the gravitational waves. The sideband frequency being high may result in undesirable noise at the photo-detection. For example, these parameters assume that the asymmetry length is 0.824 m and $f_2 = 182$ MHz in our simulation for LCGT (see table 2).

The second benefit of the coupled-reflected method is that the clean l_- signals can be acquired at the DP. In general, L_- and l_- should be isolated from L_+, l_+ and l_s signals as much as possible, because L_- and l_- may include the gravitational-wave signals and the two signals cannot be separately extracted in principle. The coupled-reflected method allows the l_- signals without admixture of l_+ and l_s because there are no AM sidebands in the SEC owing to the condition of $r_{MI2} = -1$.

Another major advantage of the coupled-reflected method is that the delocation technique can diagonalize the sensing matrix optically. When one of the l_+, l_- and l_s signals is extracted, two kinds of demodulation phases can be chosen so that one desired signal is maximized, or an undesired signal is minimized. The l_+, l_- and l_s signals are superposing in the demodulation-phase domain and cannot be extracted individually. Especially, the l_+ and l_s signals have the exact same dependences on the demodulation phases. The delocation scheme can avoid this degeneracy. The delocation is a macroscopic detuning for the AM sidebands by changing the position of the PRM. The off-resonant AM fields can change the optimum double-demodulation phases for the three signals. The appropriate delocation amount realizes that one desired signal can be extracted while the undesired signals are zero on a pair of appropriate delocation phases. Therefore, the exact diagonalization of the sensing matrix is possible when optimum demodulation phases are chosen. Although the PRM position change affects the resonant condition of the PM sideband field in the PRC as well as the AM sidebands, the PM sidebands are only slightly off-resonant since the delocation phase for the PM sidebands is small. This is because the delocation phase is proportional to the sideband frequencies and f_1 is much smaller than f_2. See equation (18) in section 5.

The delocation technique seems to decrease about 40% of signal compared with no delocation. This is because they are displaced from its resonant point and the power of AM sideband fields is reduced in the PRC.

4. Relation to other schemes

The coupled-reflected method was derived from three control schemes for the RSE interferometer which has already been discussed, or has been tested by prototype interferometers. The schemes can be categorized from the viewpoint of the sideband options. Depicted in figure 4, each set of sidebands has two options: for PM sidebands, the critically coupled or the complete transmission through the MI; for AM sidebands, the complete reflection or the quasi-reflection by the MI. The combination of these options derives four schemes: the transmitted-quasi reflected method, the critically coupled-quasi reflected method, the transmitted-reflected method and the critically coupled-reflected method. The critically coupled-reflected method was inspired as the fourth panel of the table shown in figure 4(*d*).

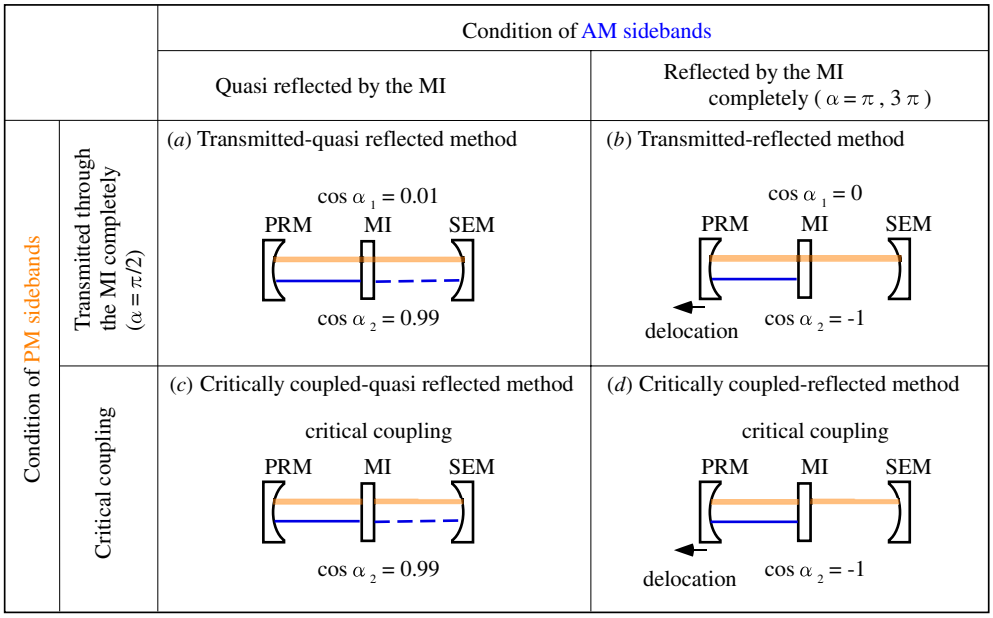

Figure 4. Relation of four signal sensing and control schemes. They are categorized by the optical conditions of the sidebands in the PRC and section. The PM sidebands (shown as upper lines in the cavity, or in orange in the web version) are critically coupled or they transmit through the MI. The AM sidebands (shown as lower lines in the cavity, or in blue in the web version) are quasi-reflected or completely reflected by the MI. The combinations of these conditions provide the four schemes.

The transmitted-quasi reflected method was developed by the LIGO group as a default method for Advanced LIGO [10]. As is shown in figure 4(*a*), almost all of the PM sidebands transmit the MI. The frequency of the PM sidebands which satisfies $r_{\rm com} = -r_{\rm p}$ is adopted for this method. On the other hand, a great part of the AM sidebands is reflected by the MI. The PM sidebands resonate both in the PRC and in the section, and the AM sidebands resonate only in the PRC. It is noted that the original scheme was not exactly the same as the transmitted-quasi reflected method, but essentially equivalent to it. The original method for Advanced LIGO was to use two sets of PM sidebands instead of AM and the carrier field is detuned in the SEC since Advanced LIGO is a detuned RSE interferometer.

The transmitted-reflected method has been developed by Sato as the control scheme for LCGT [9]. As shown in figure 4(*b*), the PM sidebands pass through the MI completely and all the AM sidebands are reflected by the MI. The MI asymmetry length and the sideband frequencies satisfy $\cos\alpha_1 = 0, \cos\alpha_2 = -1$ [5] so that the sideband conditions are met. The delocation technique is first introduced with this method.

The critically coupled-quasi reflected method has already been tested by Somiya [11]. As is shown in figure 4(*c*), the PM sidebands are critically coupled and the AM sidebands slightly reach the SEM. The critical coupling condition was first introduced with a method to maximize $l_{\rm s}$ signals by this method.

Comparing these four methods, one can find that the coupled-reflected method inherits the advantages of other methods: a short asymmetry length of MI can be available inheriting the advantage of the critically coupled-quasi reflected method; no cross-talk between L_+, l_+

[5] When $r_{\rm p} = r_{\rm s}$, the critical coupling condition for PM sidebands is satisfied in this method as well.

and l_s in the l_- signals at the DP inherits the advantage of the transmitted-reflected method; the diagonalized length sensing matrix by the delocation technique inherits the advantage of the transmitted-reflected method as well. In the following section, the analytical expressions and the numerical simulation results of the coupled-reflected method will be shown.

5. Control signals and simulation result

The transfer function of light fields from the input to an arbitrary port is expressed as

$$T = \frac{E}{E_{\rm in}}, \tag{10}$$

where $E_{\rm in}$ is the light field of the incident beam and E is the light field at the port. $E_{\rm in}$ contains the carrier component and two sets of upper (U) and lower (L) sideband components which are generated by the EOMs. The transfer function at the PO is

$$T_j = \frac{t_{\rm p}}{1 - r_{\rm p} R_j \, {\rm e}^{-{\rm i}\phi_{{\rm p}j}}}, \tag{11}$$

where $j = 1, 2$ for the PM and AM sidebands, respectively and $\phi_{{\rm p}j}$ is the round trip phase in the PRC. $R_j (j = 1, 2)$ is the reflectivity of the compound cavity which includes the MI, FP arms and SEC for the PM and AM sidebands, respectively;

$$R_j = r_{{\rm cav}\,j} \left[{\rm e}^{-{\rm i}\phi_{\rm avr}} \cos\alpha_j - \frac{{\rm e}^{-2i\phi_{\rm avr}} \sin^2\alpha_j r_{\rm s} r_{{\rm cav}\,j} \, {\rm e}^{-{\rm i}\phi_{{\rm s}j}}}{1 - r_{\rm s} r_{{\rm cav}\,j} \cos\alpha_j \, {\rm e}^{-{\rm i}\phi_{\rm avr}} \, {\rm e}^{-{\rm i}\phi_{{\rm s}j}}} \right], \tag{12}$$

where $\phi_{\rm avr}$ is the average round trip phase of l_1 and l_2 and $r_{{\rm cav}\,j}$ is the compound reflectivity of the arm cavity for each sideband component.

The sensitivities of the double-demodulated signals at the PO, $V_{\rm PO}$ for l_k ($k = +, -, {\rm p}$) are given as

$$\frac{\partial V_{\rm PO}}{\partial l_k} = \frac{\partial}{\partial l_k} {\rm Re}\left[\left\{ T_{\rm U1} T^*_{\rm L2} + T^*_{\rm L1} T_{\rm U2} \right\} {\rm e}^{-{\rm i}(\delta 1 + \delta 2)} + \left\{ T^*_{\rm U1} T_{\rm U2} + T_{\rm L1} T^*_{\rm L2} \right\} {\rm e}^{-{\rm i}(\delta 1 - \delta 2)} \right], \tag{13}$$

where $T_{\rm U1(L1)}$ represents the transfer functions of upper (lower) PM sidebands and $T_{\rm U2(L2)}$ is the transfer functions of AM sidebands at the PO. $\delta 1$ and $\delta 2$ are the demodulation phases.

From equations (11) and (13), the sensitivities of $V_{\rm PO}$ for l_+, l_- and $l_{\rm s}$ are

$$\frac{\partial V_{\rm PO}}{\partial l_+} \propto {\rm Im}[{\rm i} g_1 \, {\rm e}^{-{\rm i}\delta_1}] \, {\rm Re}\left[-g_2^2 R_2 \, {\rm e}^{-{\rm i}\triangle_{\rm p2}} \, {\rm e}^{-{\rm i}\delta_2} \right] + {\rm Re}\left[g_1^2 R_1 \, {\rm e}^{-{\rm i}\triangle_{\rm p1}} \, {\rm e}^{-{\rm i}\delta_1} \right] {\rm Re}[g_2 \, {\rm e}^{-{\rm i}\delta_2}] \tag{14}$$

$$\frac{\partial V_{\rm PO}}{\partial l_-} \propto {\rm Re}\left[{\rm i} g_1^2 \, {\rm e}^{-{\rm i}\triangle_{\rm p1}} \, {\rm e}^{-{\rm i}\delta_1} \right] {\rm Re}[g_2 \, {\rm e}^{-{\rm i}\delta_2}] \tag{15}$$

$$\frac{\partial V_{\rm PO}}{\partial l_{\rm s}} \propto -{\rm Re}\left[g_1^2 \, {\rm e}^{-{\rm i}\triangle_{\rm p1}} \, {\rm e}^{-{\rm i}\delta_1} \right] {\rm Re}[g_2 \, {\rm e}^{-{\rm i}\delta_2}] \tag{16}$$

where g_j is a square root of the power recycling gain for each sideband,

$$g_j = \frac{t_{\rm p}}{1 - r_{\rm p} R_j \, {\rm e}^{-{\rm i}\triangle_{{\rm p}j}}} \tag{17}$$

$$\triangle_{{\rm p}j} = \frac{2\pi f_j l_{\rm del}}{c}. \tag{18}$$

These equations include the effect of the delocation. The sidebands undergo delocation phase shifts, $\triangle_{{\rm p}j}$, caused by the macroscopic length displacement, $l_{\rm del}$, from the resonant point of the

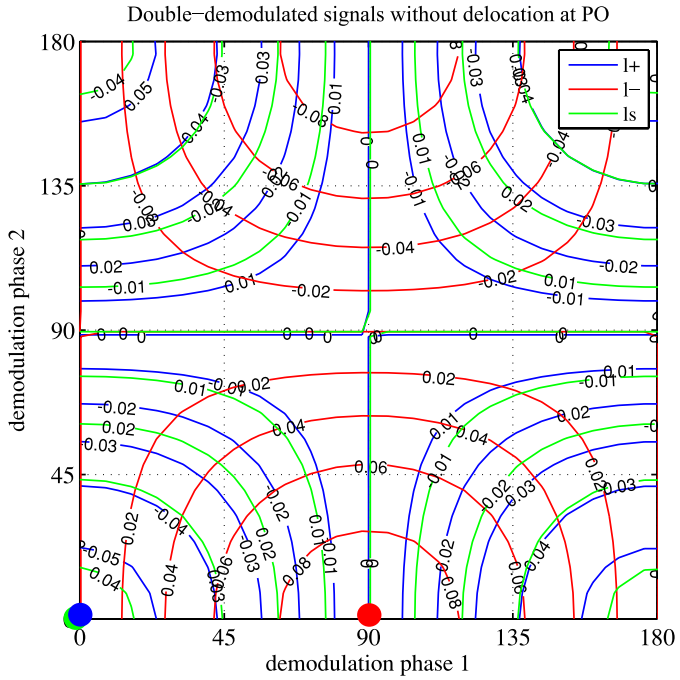

Figure 5. Contour map of l_+, l_- and l_s signals when the delocation is not applied. The three dots represent the maximum points for the three signals. At any demodulation phase coordinate, the maximum points of l_+ and l_s completely overlap. They cannot be extracted separately by choosing any demodulation phase.

PRC. The two sideband fields experience different phase shifts because their phase changes depend on both the sideband frequencies and the displacement length. The SEC does not experience any change by the delocation.

When the delocation is not applied, and both the sidebands resonate in the PRC, $\triangle_{\mathrm{p1}} = \triangle_{\mathrm{p2}} = 0$. Therefore the signals without the delocation are

$$\frac{\partial V_{\mathrm{PO}}}{\partial l_+} \propto \cos\delta 1 \cos\delta 2 \tag{19}$$

$$\frac{\partial V_{\mathrm{PO}}}{\partial l_-} \propto \sin\delta 1 \cos\delta 2 \tag{20}$$

$$\frac{\partial V_{\mathrm{PO}}}{\partial l_{\mathrm{s}}} \propto \cos\delta 1 \cos\delta 2, \tag{21}$$

equations (19) and (21) indicate that l_+ and l_{s} are exactly overlapping on the δ_1–δ_2 plane. The demodulation phases for both l_+ and l_{s} are $(\delta_1, \delta_2) = (0, 0)$ to maximize the signals. Therefore, the two signals cannot be extracted separately by choosing any demodulation phases. On the other hand, the l_- signal can be extracted at the maximal point, $(\delta_1, \delta_2) = (\pi/2, 0)$ where the other two signals are zero. The contour plots for these signals are shown in figure 5.

When the delocation is applied, $\triangle_{\mathrm{p1}}$ and $\triangle_{\mathrm{p2}}$ are nonzero. These nonzero terms change the signal dependences on δ_j and they can solve the signal degeneracy. Depicted in figure 6, only one signal can be extracted without mixing with others by choosing appropriate demodulation

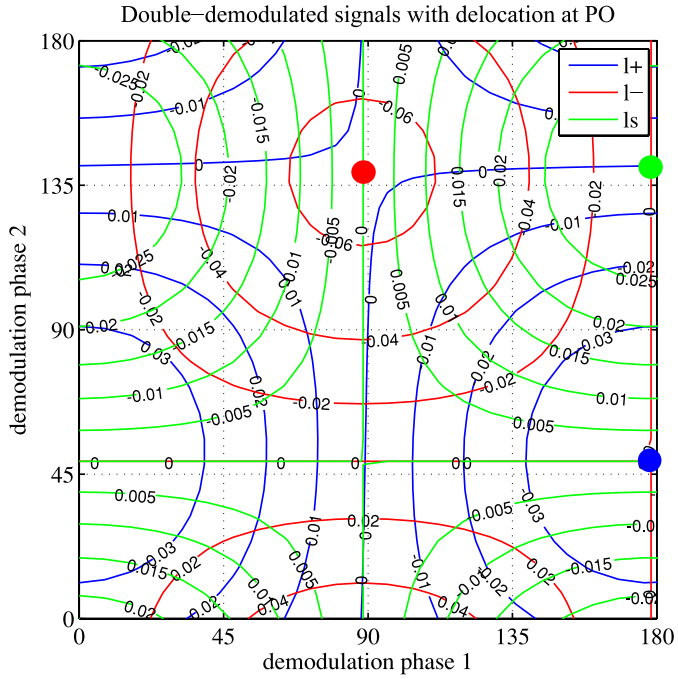

Figure 6. Contour map of l_+, l_- and l_s signals when the delocation is not applied. The PRM is displaced an appropriate amount from the resonant point. The delocation length is adjusted so that undesired signals are almost zero at each maximum point of l_+, l_- and l_s. The three signals can be extracted separately at their optimum demodulation phases.

Table 2. The numerical results of the length-sensing matrix with the coupled-reflected method. Five signals are extracted from each port, using the demodulation scheme. The important feature is that the l_+, l_- and l_s signals are almost separated at the appropriate pairs of demodulation phases ($\delta 1$ and $\delta 2$). We used the preliminary parameter for LCGT; $r_p = 0.894$, $r_s = 0.878$. According to these reflectivities, the asymmetry length $\Delta\ell = 0.824$ m and the sideband frequencies of $f_1 = 7$ MHz and $f_2 = 182$ MHz were chosen. For simplicity, the interferometer was assumed to be lossless. The delocation length was 0.014m which corresponds to $\triangle_{p2} = 3.06^\circ$. This numerical simulation was done by FINESSE software.

Length sensing matrix							
Port	$\delta 1$	$\delta 2$	L_+	L_-	l_+	l_-	l_s
PO	0		1	3.83×10^{-8}	-4.25×10^{-4}	3.52×10^{-5}	5.08×10^{-4}
DP	0		-4.65×10^{-12}	1	-1.55×10^{-18}	1.00×10^{-3}	1.55×10^{-18}
PO	178	49.0	-1.23×10^{-3}	2.55×10^{-8}	1	2.25×10^{-7}	-2.41×10^{-5}
DP	0	136	4.65×10^{-4}	1.24×10^{-3}	-3.77×10^{-6}	1	-3.89×10^{-9}
PO	178	141	1.26×10^{-3}	-1.79×10^{-8}	8.67×10^{-7}	5.67×10^{-7}	1

phases; for example, l_+ becomes maximum whereas l_s is zero on a certain pair of demodulation phases with a suitable amount of delocation.

Table 2 shows the matrix of the length sensing signals. The demodulation phases are optimized to remove undesired signal components. E.g., the L_+ signal is extracted at the PO

by the single demodulation on a demodulation phase 0 whereas the other four signals are contained. This simulation was done by FINESSE [12].

This well-diagonalized sensing matrix is supposed to provide the robust control because the optical diagonalization enables the servo loop to be simple. Even without the signal diagonalization, the interferometer can be controlled by using a signal matrix which has off-diagonal elements. But in this case, some additional servo systems are necessary to compensate for the off-diagonal elements. Such systems could add noise to the interferometer.

6. Summary

In summary, we have proposed a new length sensing control scheme for an RSE interferometer. The method has three significant advantages for robust control: a short asymmetry length of MI is available; the modulation sideband conditions enable the l_- to have no cross-talk between L_+, l_+ and l_s at the DP; and application of the delocation technique diagonalizes the length-sensing matrix.

Acknowledgments

This research is supported partly by a Grant-in-Aid for Scientific Research on Priority Areas (415) of the Ministry of Education, Culture, Sports, Science and Technology, from Japan and also National Science Foundation cooperative agreement no. PHY-0107417 from US funding.

References

[1] Ando M *et al* 2005 *Class. Quantum Grav.* **22** S881
[2] Acernese F *et al* 2006 *Class. Quantum Grav.* **23** S635
[3] Lück H *et al* 2006 *Class. Quantum Grav.* **21** S71
[4] Abramovici A *et al* 1992 *Science* **256** 325
[5] Sigg D *et al* 2006 *Class. Quantum Grav.* **23** S51
[6] Kuroda K *et al* 2006 *Class. Quantum Grav.* **23** S215
[7] Weinstein A *et al* 2002 *Class. Quantum Grav.* **19** S1575
[8] Mizuno J, Strain K A, Nelson P G, Chen J M, Schilling R, Rüdiger A, Winkler W and Danzmann K 1993 *Phys. Lett.* A **175** 273
[9] Sato S, Kawamura S, Kokeyama K, Kawazoe F and Somiya K 2007 *Phys. Rev.* D **75** 082004
[10] Miyakawa O *et al* 2006 *Phys. Rev.* D **74** 022001
[11] Somiya K, Beyersdorf P, Arai K, Sato S, Kawamura S, Miyakawa O, Kawazoe F, Sakata S, Sekido A and Mio N 2005 *Appl. Opt.* **44** 16
[12] http://www.rzg.mpg.de/adf/